Local and global control of high-period unstable orbits in reversible maps

Yu. L. Bolotin,[1] V. Yu.Gonchar,[1] A. A. Krokhin,[2] P. H. Hernández-Tejeda,[2] A. Tur,[3] and V. V. Yanovsky[1,4]
[1]*National Science Center, Kharkov Institute of Physics and Technology, Kharkov 310108, Ukraine*
[2]*Instituto de Fisica, Universidad Autonoma de Puebla, Apartado Postal J-48, Puebla 72570, Mexico*
[3]*Center D'etude Spatiale Des Rayonnements, 9 Avenue du Colonel Roche, 31028 Toulouse, France*
[4]*Institute for Single Crystals, Kharkov 310001, Ukraine*
(Received 13 October 2000; revised manuscript received 7 May 2001; published 20 July 2001)

We study the nonlinear dynamics of a complex system, described by a two-dimensional reversible map. The phase space of this map exhibits elements typical of Hamiltonian systems (stability islands) as well as of dissipative systems (attractor). Due to the interaction between the stability islands and the attractor, the transition to chaos in this system occurs through the collapse of the stability island and stochastization of the limiting-cycles orbits. We show how to apply the method of discrete parametric control to stabilize unstable high-period orbits. To achieve highly efficient control we introduce the concepts of local and global control. These concepts are useful in situations where there are ''dangerous'' points on the target orbit, i.e., the points where the probability of breakdown of control is high. As a result, the dangerous points turn out to be much more sensitive to external noise than other points on the orbit, and only the dangerous points determine how effective the control is.

DOI: 10.1103/PhysRevE.64.026218 PACS number(s): 05.45.Gg

I. INTRODUCTION

The interplay of resonances is one of the basic concepts leading to dynamical chaos in low-dimensional Hamiltonian systems [1–3]. The underlying elements of this concept have been adopted from the study of simple maps, e.g., the standard (or Chirikov) map [4,5]. In dissipative systems the origin of chaos is attributed to the existence of attractors in phase space, especially to so-called strange attractors [6,7]. Here the leading role belongs to the Henon map [8] which exhibits the most general properties of dissipative chaotic systems. A class of reversible systems that possesses properties of Hamiltonian as well as dissipative systems has been introduced in Refs. [9,10]. The phase space of a reversible system usually contains basic elements of both types: resonances and attractors. A *B* laser [11] is the first physical model where such coexistence was mentioned. The interplay between resonances and attractors in reversible systems gives rise to dynamical effects like specific bifurcations of fixed points [11–14] leading to the rearranging of the resonances and a change in the topology of a separatrix under the influence of the attractor [15,16].

In the present paper we consider a map which, according to the conventional classification [17], describes a complex system. This is a wide class of systems that even includes some biological objects. Very different systems can be included to the wide class of complex systems if they exhibit the following common features: (i) A complex system is composed of several interacting components; (ii) its phase space contains regions of regular and chaotic dynamics; (iii) it exhibits a multiscale spatiotemporal behavior [17]. Because of the presence of different components, it is expected that even a weak perturbation induces transitions between them. In this case one can formulate a problem of control of the dynamics of the complex system. The dynamics in complex systems can be controlled by the methods similar to those proposed in Refs. [18–20]. The general idea of these methods is to optimize the dynamics and to obtain the desired behavior by applying an intentional small perturbation to the system. As a result, chaotic oscillations are transformed into periodic ones. It is assumed that the perturbation, being weak, does not change the topology of the phase space.

In this paper we demonstrate the effectiveness of discrete parametric control for the stabilization of high-period unstable orbits in the system with complex structure of the phase space. Our object of control is a two-dimensional (2D) map that describes the discrete dynamics of a linear oscillator driven by δ kicks with its stiffness coefficient proportional to the velocity [15,21]. In Sec. II we study the structure of the phase space of this map and specific effects that are due to the interaction of the attractor with the stability islands. We obtain the collapse of the stability island and study different types of transformations of fixed points of the *n*-period orbit that occur under the influence of the attractor. It is shown that in this complex system the transition to chaos does not follow the scenarios that are typical for pure dissipative or pure Hamiltonian systems. For large values of the nonlinearity parameter we obtain a regime of strong stochastization. This regime is characterized by exponential sensitivity to the initial conditions when a trajectory approaches the limiting cycles, i.e., attractor or infinity. In Sec. III we show how to apply the method of discrete parametric control to stabilize high-period unstable orbits. In the control of a complex system one faces a difficulty that originates from the presence of the attractor. The properties of those points on the unstable orbit that are close to the attractor are very different from the properties of all other points. In particular, we show that some characteristics of the unstable periodic orbits (UPO) which are responsible for the effectiveness of control differ along the orbit by 4 orders of magnitude. Because of such a marked lack of homogeniety it is worthwhile to introduce *local* and *global* control. We also study the stability of the control with respect to external

 ©2001 The American Physical Society

Gaussian noise. Here we determine the *dangerous* points on the unstable orbit. These are the points where the probability of breakdown of control is much higher than the mean value. By introducing the concept of local and global controls, we develop an effective and practical strategy of stabilization of the UPO.

II. GENERAL DYNAMICAL ANALYSIS OF THE MAP

We consider a map

$$\mathbf{r}_{n+1}=\begin{pmatrix} x_{n+1} \\ y_{n+1} \end{pmatrix}=\mathbf{F}(\mathbf{r}_n)=\mathbf{F}\begin{pmatrix} x_n \\ y_n \end{pmatrix}=\begin{pmatrix} x_n+y_{n+1}(\mathrm{mod}\,2) \\ y_n-\varepsilon(a-y_n)x_n \end{pmatrix}, \tag{1}$$

which describes the evolution of a complex system. Using the second of Eq. (1), the coordinate y_{n+1} in the right-hand side of the first equation can be expressed through x_n and y_n, thus giving the explicit form of the transformation $\binom{x_n}{y_n} \to \binom{x_{n+1}}{y_{n+1}}$. In what follows we show that the phase space of this map contains elements of Hamiltonian as well as of dissipative systems. The phase space of this map is a surface of a cylinder $R\times S$, where $x\in[-1,1]$; points $x=+1$ and $x=-1$ are identical. Variable x_n plays the role of an angular coordinate. The map (1) has fixed points $P_k^s=(x_k^s,y_k^s)$, where $x_k^s=0$ and $y_k^s=2k(k=\pm1,\pm2,\ldots,\quad a\neq 2k)$. For given values of the parameters ϵ and a, two solutions of a characteristic equation

$$\lambda^2+\lambda\,\mathrm{tr}\,\mathbf{L}+\det\mathbf{L}=0 \tag{2}$$

determine the type of a fixed point. Here $\mathbf{L}(\mathbf{r}_k)=(\partial\mathbf{F}/\partial\mathbf{r})|_{\mathbf{r}=\mathbf{r}_k}$ is the Jacobian matrix of the map Eq. (1). It is obtained as a result of linearization of Eq. (1) in the vicinity of a fixed point. Straightforward calculations of $\mathrm{tr}\,\mathbf{L}$ and $\det\mathbf{L}$ give

$$\det\mathbf{L}=1,\quad \mathrm{tr}\,\mathbf{L}=2-\epsilon(a-y_k^s). \tag{3}$$

A standard classification of fixed points by values of $\mathrm{tr}\,\mathbf{L}$ and $\det\mathbf{L}$ is shown in a compact form in Fig. 1. The condition $\det\mathbf{L}=1$ means that there are only hyperbolic (saddle) or elliptic (center) fixed points (see Fig. 1), i.e., those that exist in Hamiltonian or conservative systems. In Fig. 2 we display the domains of hyperbolic and elliptic points in the plane of parameters (ρ_k,ϵ), where $\rho_k\equiv a-y_k^s$ is the distance from the attractor to the kth fixed point. A hyperbola $\rho_k=4/\epsilon$ separates the domains of elliptic and hyperbolic points.

Another important element of the phase portrait of the mapping (1) is an invariant manifold which defines for any parameter ϵ a family of special *exact* solutions

$$x_{n+1}=(x_n+a),\quad y_n=a(\mathrm{mod}2). \tag{4}$$

At fixed a each solution gives a periodic or quasiperiodic trajectory for rational or irrational values of a, respectively. Different solutions of Eq. (4) are discriminated by the initial conditions x_0. After one iteration a point at the special trajectory (4) rotates by an angle πa and the coordinate y is unchanged. Hence the parameter $\nu=a/2$ plays the role of a winding number [2,22]. If $\epsilon<1$ the close-lying trajectories converge to the corresponding special solution (4) $y_n=a$. Then it is an attractor. The size of the attractor's basin is determined by the parameter ϵ. The border of the basin has a complicated fractal structure for $\epsilon>1$. The position and structure of the attractor are determined only by the parameter a. If $\nu=a/2$ is rational, $\nu=p/q$ (p and q are mutually coprime numbers), the attractor consists of periodic trajectories with period q, and of quasiperiodic trajectories otherwise.

For a particular case of $a=2k$ $(k=0,\pm1,\pm2,\ldots)$ the y coordinate of the attractor coincides with one of the above-mentioned fixed points, y_k^s. In this case the attractor consists only of the fixed points of the map (4).

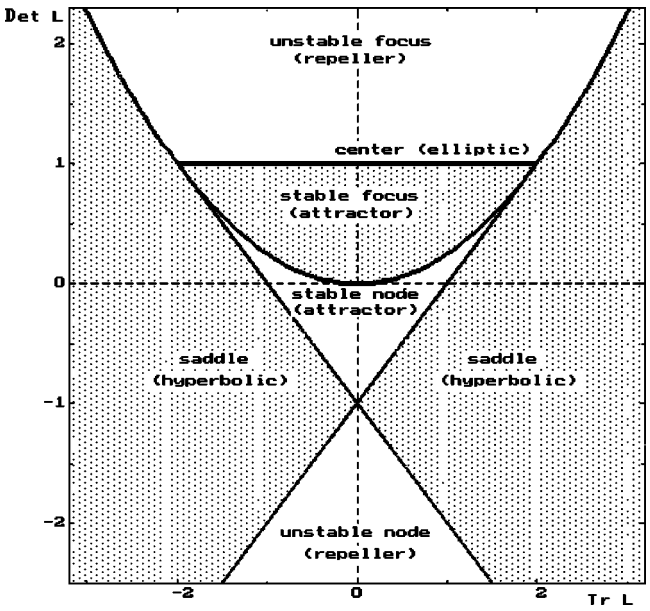

FIG. 1. Classification of fixed points according to the values of $\det\mathbf{L}$ and $\mathrm{tr}\,\mathbf{L}$.

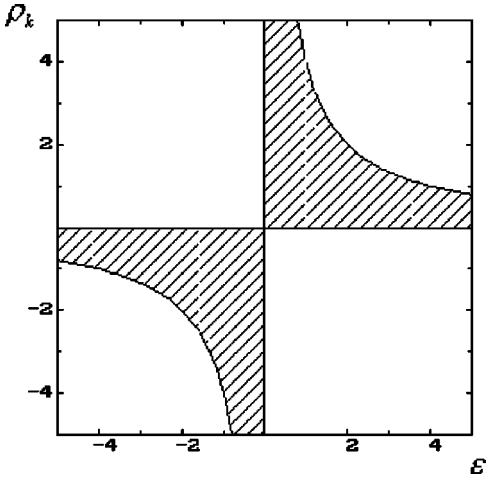

FIG. 2. Domains in the (ρ_k,ϵ) plane containing elliptic (hatched region) or hyperbolic (blank region) fixed points. These domains are separated by the curve $\epsilon\rho_k=4$.

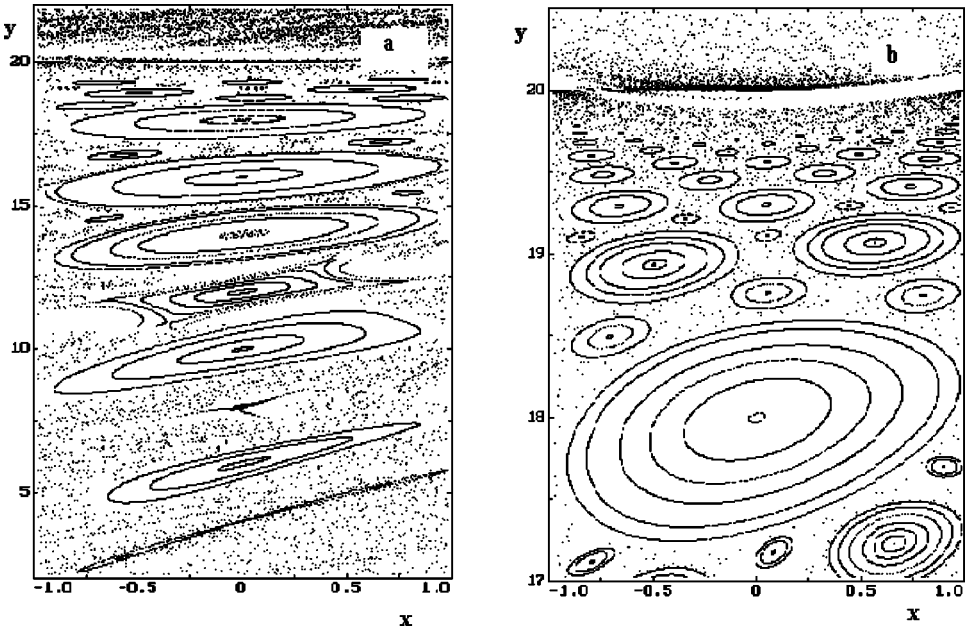

FIG. 3. (a) Phase space of the mapping Eq. (1) for $a=20$ and $\epsilon=0.2515$. (b) Enlargement of the region of the phase space containing stability islands of higher orders.

For small values of ϵ the trajectories approach the attractor at an exponential rate, $\langle (y_i-a)\rangle \approx e^{-\gamma N}$ [angular brackets denote averaging over the trajectory, $\langle f_i\rangle=(1/N)\Sigma_{i=1}^{N} f_i$]. To demonstrate this property we represent the first equation of the map (1) in the equivalent form $(y_{n+1}-a)=(y_n-a)(1+\epsilon x_n)$. Iterating this equation we obtain a formal solution,

$$(y_{n+1}-a)=(y_0-a)\prod_{i=0}^{n}(1+\epsilon x_i). \tag{5}$$

Rewriting the product in exponential form,

$$\prod_{i=0}^{n}(1+\epsilon x_i)=\exp\left[(n+1)\frac{\sum_{i=0}^{n}\ln(1+\epsilon x_i)}{n+1}\right]\equiv\exp[(n+1)\times\langle\ln(1+\epsilon x)\rangle], \tag{6}$$

and replacing the time average by a space average (due to ergodicity), we get

$$\begin{aligned}\gamma&=\langle\ln(1+\epsilon x)\rangle\\&=\frac{1}{2}\int_{-1}^{1}\ln(1+\epsilon x)\,dx\\&=\frac{(1+\epsilon)\ln(1+\epsilon)-(1-\epsilon)\ln(1-\epsilon)}{2\epsilon}-1.\end{aligned} \tag{7}$$

In the limiting case $\epsilon\ll 1$ the rate γ is reduced to

$$\gamma\approx\frac{\epsilon^2}{6}. \tag{8}$$

The nonzero rate of attraction γ appears in the second order with ϵ. The linear term vanishes because attraction alternates with repulsion each half-period.

Variations of the parameters a and ϵ may lead to transformations of the fixed points of the map (1), $P_k^s=(y_k^s=2k, x_k^s=0)$, of one type to another. A general classification of the fixed points of the map (1) is shown in Fig. 1, which we will use in order to follow these transformations. Let us describe a typical phase portrait of the map Eq. (1). Figure 3 shows the phase space for $a=20$ and $\varepsilon=0.2515$. The attractor (4) is located on the line $y=a$. If $\epsilon>0$ only hyperbolic fixed points (saddles) are located above the attractor located at $y>a$. According to Fig. 2, elliptic fixed points (centers) are squeezed within the interval $0<\rho_k<4/\varepsilon$, i.e., $a-4/\epsilon<y<a$. Each center, surrounded by periodic trajectories, forms a stability island (see Fig. 3). There are only hyperbolic fixed points (saddles) below the line $y=a-4/\epsilon$. The width of the zone where the elliptic fixed points are placed depends on ϵ. When the parameter ϵ increases the zone of elliptic points, $a-4/\epsilon<y<a$ narrows. This zone vanishes when the horizontal line $y=a-4/\epsilon$ crosses nearest to the attractor fixed point. At that value of ϵ all the fixed points become hyperbolic. For $\epsilon<0$ (see Fig. 2), elliptic centers lie within the interval $a<y<a-4/\epsilon$ and hyperbolic saddles lie outside it. Due to this symmetry, we can analyze the phase portrait only for the case $\epsilon>0$.

Since the position of the attractor (along the y axis) depends on the variable parameter a, the influence of the attractor on the fixed points can be easily studied. Varying a one can shift the attractor and thus observe the corresponding changes that occur with the fixed points. Using Fig. 2 one can analyze how the type of fixed point changes when the attractor approaches it. Suppose that for a given $\epsilon>0$ the attractor is located above the fixed point at a distance $\rho_k \gg 4/\epsilon$ away from it. According to the classification shown in Fig. 2 this point is a hyperbolic one. When the attractor approaches the fixed point, a bifurcation occurs and it is converted into an elliptic one at $\rho_k=4/\epsilon$. Then this point remains elliptic until the attractor collides with it. At that moment the elliptic point changes back into the hyperbolic one. When the

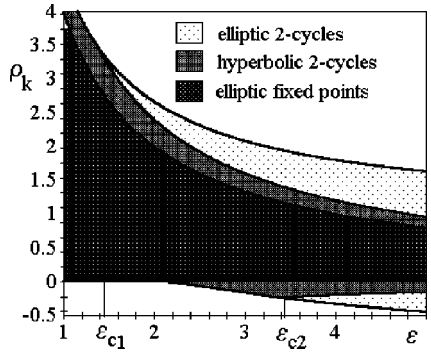

FIG. 4. Hatched regions show the domains of existence of two-cycles and fixed points in the ϵ,ρ_k plane.

attractor moves down to the region of negative y, the point remains hyperbolic. Thus it is possible to separate local and nonlocal influences of the attractor on the fixed point. The local effect manifests itself when the attractor collides with the fixed point. The nonlocal influence manifests itself through the bifurcation, when the attractor is at the critical distance $4/\epsilon$ away from the fixed point.

Apart from the fixed points there are periodic orbits in the phase portrait of the map (1). In what follows we will analyze the conditions when the orbits with the shortest period (period-2 or two-cycle orbits) exist and study the transformations of the two-cycle orbits with variations of the parameters a and ϵ. Such analysis is necessary for a complete description of the bifurcations of the fixed points. Since a two-cycle orbit involves two steps of iterations of the map (1), the stability matrix of a two-cycle orbit is given by $\mathbf{L}^2=\mathbf{L}(\mathbf{r}_2)\mathbf{L}(\mathbf{r}_1)$. Omitting simple algebra, we represent the results in Fig. 4 where we show the transformations of two-cycle orbits in the (ϵ,ρ_k) plane.

A period-2 orbit consists of two points $\mathbf{Z}_1=(y_1,x_1)$ and $\mathbf{Z}_2=(y_2,x_2)$ which are transformed into each other after one iteration, $\mathbf{Z}_{1,2}=\mathbf{F}(\mathbf{Z}_{2,1})$. A period-2 orbit consists of two points $\mathbf{Z}_1=(x_1,y_1)$ and $\mathbf{Z}_2=(x_2,y_2)$ which are changed into each other after one iteration, $\mathbf{Z}_{1,2}=\mathbf{F}(\mathbf{Z}_{2,1})$. The size of the period-2 orbit is the distance between $\mathbf{Z}_1$ and $\mathbf{Z}_2$. Let us analyze first the nonlocal influence of the attractor on the fixed point. Suppose that in the case $\epsilon>\epsilon_{c1}=\sqrt{2}$ the attractor is located far away from a hyperbolic fixed point. When the attractor is approaching the fixed point, the period-2 orbit of a *finite* size $[|x_1-x_2|=\frac{1}{2}|y_1-y_2|=(2+\epsilon)/(1+\epsilon)]$ appears in the vicinity of this fixed point when the attractor and the fixed point draw together up to the distance $\rho_k=(2+\epsilon)^2/\epsilon(1+\epsilon)$. The orbit remains a hyperbolic one until the distance decreases to the value $\rho_k=2(1+\sqrt{2})/\epsilon$. Here the orbit becomes elliptic and its characteristic size shrinks. The next qualitative transition takes place at $\rho_k=4/\epsilon$. Here the elliptic period-2 orbit vanishes at the moment when the hyperbolic fixed point becomes elliptic. A similar scenario of the nonlocal influence is also realized for the case $0<\epsilon<\sqrt{2}$. The only difference is the absence of the stage corresponding to the hyperbolic period-2 orbit (see Fig. 4). A bifurcation of the fixed point due to the nonlocal attractor's influence is shown in Fig. 5(a).

Let us proceed to the case of the local influence when the

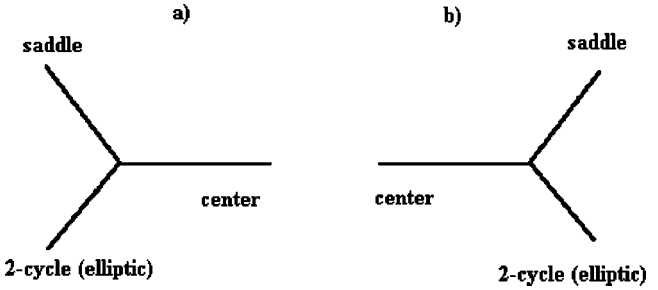

FIG. 5. Bifurcations of the fixed point when the attractor is approaching it for (a) nonlocal and (b) local.

attractor crosses the elliptic fixed point and first consider the range of parameters $\epsilon>\epsilon_{c2}=2+\sqrt{2}$, see Fig. 4. When the attractor collides with the elliptic fixed point it is transformed into a hyperbolic one. At the same moment the elliptic period-2 orbit emerges. Unlike the nonlocal case, the size of this orbit increases gradually from zero. While the attractor moves to the negative y plane, the period-2 orbit becomes wider and at $\rho_k=2(1-\sqrt{2})/\epsilon$ the period-2 elliptic orbit becomes hyperbolic. This hyperbolic point disappears at $\rho_k=(2-\epsilon)^2/\epsilon(1-\epsilon)$. In the case $2<\epsilon<\epsilon_{c2}$ the evolution of the period-2 orbit is the same except that the stage of the hyperbolic orbit is absent, see Fig. 4. The local influence of the attractor is shown in Fig. 5(b). The evolution of the period-2 orbit for the reverse motion of the attractor occurs as it is shown in Fig. 5(a) (local influence) and Fig. 5(b) (nonlocal influence). No other types of bifurcations are expected to appear under either local or nonlocal influence of the attractor on the fixed points. The numerical study is in complete agreement with the aforementioned analysis.

The chaotic dynamics of map (1) reveals peculiarities that do not exist in pure Hamiltonian or pure dissipative systems. For example, in the case $\epsilon<1$ the chaotic regime has an intermediate character. The trajectories from the stochastic layer approach the attractor where their flux becomes regular. If the attractor approaches the stability island sufficiently the profile of the boundary of the stochastic layer repeats the shape of the boundary of the attractor. The trajectory remains a very short time near the attractor. In this region the shape of the trajectory is flat, i.e., its y coordinate is almost constant. Away from the attractor the trajectory is chaotic with a rather large amplitude of chaotic oscillations along axis y. It executes chaotic oscillations until it returns to the attractor again. This type of motion can be compared to the so-called intermittency [23] which is well studied in 1D maps. Such behavior is observed in the interval $a>y>a-4/\epsilon$. Since there are only hyperbolic points, the stability islands do not appear. In the cylindrical phase space the unstable branches of these fixed points wind around the cylinder and approach eventually $\pm\infty$ along the y axis. There they form a complicated structure of stochastic trajectories.

When ϵ increases and exceeds one, the invariant manifold Eq. (4) does not attract trajectories any more. Then the attractor disappears; the invariant manifold, however, does not. Since the attractive properties of the invariant manifold are lost, this leads to instability in the trajectories. The diffusive motion along the y axis becomes anomalous, with a high

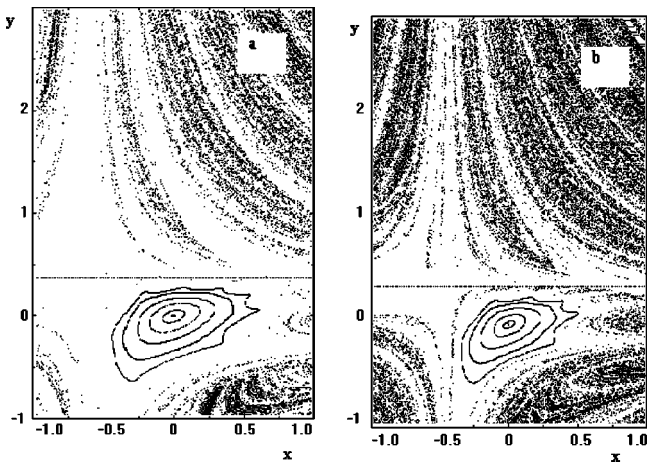

FIG. 6. Structure of the phase space for $a=2.5$ and (a) $\varepsilon=1.7$, (b) $\varepsilon=2.2$. In the vicinity of each black dot the motion is regular ($\lambda<-0.1$). Blank regions correspond to chaotic motion ($\lambda>0.1$).

intermittency of the trajectories. For example, a trajectory which slowly diffuses away from the attractor to $y=+\infty$ suddenly makes an abrupt jump to the region below the attractor. This happens when one of the factors on the right-hand side of Eq. (5) changes its sign, thus leading to a giant instant displacement along the y axis. Making use of Eq. (5) we can evaluate the mean deviation of the anomalous trajectory from the attractor,

$$\langle (y_{n+1}-a)^2\rangle=(y_0-a)^2(1+2\epsilon\langle x\rangle+\epsilon^2\langle x^2\rangle)^n. \qquad (9)$$

Here we assume that the coordinates x_i and x_j are uncorrelated, i.e., $\langle x_i x_j\rangle\propto\delta_{ij}$ because of the chaotic nature of the trajectory. Finite correlations lead to some minor changes only. Taking into account that for a homogeneous trajectory $\langle x\rangle=0$ and $\langle x^2\rangle=1/3$, we get

$$\langle \rho_{n+1}^2\rangle=\langle (y_{n+1}-a)^2\rangle=(y_0-a)^2\exp[n\ln(1+\epsilon^2/3)]. \qquad (10)$$

Thus $\langle\rho_n^2\rangle$ grows exponentially, unlike a normal diffusive regime where $\langle\rho_n^2\rangle\propto n$.

In general, to distinguish the areas with regular and chaotic dynamics, we calculate the Lyapunov exponents [1]. We classify the domains of the phase space according to the sign of the local Lyapunov exponent λ calculated for a pair of neighboring trajectories. Then, marking the domains of regular and chaotic motion where, respectively, $\lambda<-0.1$ or $\lambda>0.1$ with black and white dots, we visualize the structure of the phase space. The typical pattern for $a=2.5$, $\epsilon=1.7$ is shown in Fig. 6(a). The solid line shows the island of stability, located in the area of irregular dynamics. For larger ϵ the measure of chaos increases, see Fig. 6(b) for $\epsilon=2.2$. These figures demonstrate a complex fractal structure of the phase space. Initial points of the regular and chaotic trajectories cover the phase space, forming a stochastic fractal pattern. We would like to mention a correlation between this pattern and the fractal structure of the attractor's basin. This correlation originates from the fact that the basin contains mainly the regular trajectories. Because of strong chaos one cannot predict even the asymptotic behavior (regular or chaotic) of a trajectory at $t\to\infty$, nor its final point, $y=a$ or $y=\pm\infty$.

A simple modification of the map (1) allows one to change the level of dissipation. This is done by introducing a coefficient $(1-c)$ at the term y_n in the first equation of the set (1). When the dissipation is switched on smoothly (c increases from 0 to 1) , the Hamiltonian component is suppressed and the system exhibits a strange attractor via a cascade of bifurcations.

The above analysis suggests that due to the peculiarities of the dynamics of the complex system (1) one can expect certain difficulties in controlling the unstable periodic orbits. Below we will demonstrate that in order to develop an effective method of control one needs to take into account the presence of the attractor and the stability islands, inhomogeneity and the complex structure of the phase space, and the anomalous diffusion of the trajectories.

III. LOCAL AND GLOBAL CONTROL OF THE UNSTABLE PERIODIC ORBIT

In what follows we apply the discrete one-parametric Otto, Grebogi, and Yorke (OGY) method [18] in order to control the high-period unstable orbits of the map (1). The method was originally proposed to stabilize UPO imbedded within a strange attractor. Later it was generalized for the case of Hamiltonian systems [19]. Different modifications and numerous applications of the OGY method can be found in Ref. [20].

Let the orbit to be controlled follow a periodic sequence: $\mathbf{r}_1^*\to\mathbf{r}_2^*\to\cdots\to\mathbf{r}_k^*\to\mathbf{r}_{k+1}^*=\mathbf{r}_1^*$. Linearizing the dynamical equations (1) in the neighborhood of this periodic orbit $\mathbf{r}_n^*(p_0)$, we obtain

$$\mathbf{r}_{n+1}-\mathbf{r}_{n+1}^*(p_0)=\mathbf{L}[\mathbf{r}_n-\mathbf{r}_n^*(p_0)]+\mathbf{B}\delta p_n, \qquad (11)$$

where $\mathbf{B}=(\partial/\partial p)\mathbf{F}(r_n^*,p)|_{p=p_0}$, parameter p is either a or ϵ, and p_0 is its nominal value. Control is achieved by small variations of the parameter p.

A direct application of the OGY method for the control of the UPO faces two difficulties. First, since Eq. (1) is not a purely dissipative map, the one-step Jacobian matrix $\mathbf{L}$ may possess complex eigenvalues at some points of the orbit. This makes the application of the original OGY method impossible. To avoid this difficulty, we could apply the original OGY formula, not at each iteration, but after k iterations (one period). In other words, we could apply control for a kth power of the matrix $\mathbf{F}$ which is a cyclic matrix, $\mathbf{F}^k(\mathbf{r}_i^*)=\mathbf{r}_{i+k}^*=\mathbf{r}_i^*$ whose eigenvalues are real. However, here we face the second difficulty, namely, the sensitivity of the k-step control to external or numerical noise. A necessary modification of the OGY method that allows us to apply the parametric perturbation at each step was proposed by Lai *et al.* [24]. In their approach they considered stable and unstable directions at each point of the UPO. If $k>1$, these directions do not necessary coincide with the eigenvectors of the Jacobian matrix. An efficient method to calculate stable and unstable directions is given in Ref. [24]. They can also

be calculated by the well-known method of diagonalization of the stability matrix $\mathbf{L}^k=\mathbf{L}(\mathbf{r}_i)\mathbf{L}(\mathbf{r}_{i+1})\cdots\mathbf{L}(\mathbf{r}_{i+k})$ at each point of the orbit.

Let the unit vectors $\mathbf{e}_{s(n)}$ and $\mathbf{e}_{u(n)}$ be local ($\mathbf{r}=\mathbf{r}_n^*$) stable and unstable directions. It is worthwhile to introduce a complementary orthogonal basis $\mathbf{f}_{s(n)}$ and $\mathbf{f}_{u(n)}$ by means of the following relations: $\mathbf{f}^t_{s(n)}\mathbf{e}_{s(n)}=\mathbf{f}^t_{u(n)}\mathbf{e}_{u(n)}=1$, and $\mathbf{f}^t_{u(n)}\mathbf{e}_{s(n)}=\mathbf{f}^t_{s(n)}\mathbf{e}_{u(n)}=0$. Here index t stands for a transposed vector, $\mathbf{f}^t=(f_x,f_y)$. Making use of the OGY stabilization condition $\mathbf{f}^t_{u(n+1)}[\mathbf{r}_{n+1}-\mathbf{r}^*_{n+1}]=0$, one obtains [26]

$$\delta p_n=-\frac{\mathbf{f}^t_{u(n+1)}\{\mathbf{L}[\mathbf{r}_n-\mathbf{r}^*_n(p_0)]\}}{\mathbf{f}^t_{u(n+1)}\mathbf{B}}. \tag{12}$$

If the object of control is an unstable fixed point $\mathbf{r}^*$, then $\mathbf{f}^t_{u(n)}\to\mathbf{f}^t_u$, $\mathbf{r}^*_{(n)}\to\mathbf{r}^*$, $\mathbf{f}^t_u\mathbf{L}\to\lambda_u\mathbf{f}^t_u$. In this case Eq. (12) is reduced to the well-known OGY formula [18]. Applying the parametric perturbation (12) at each iteration, one minimizes the effect of external noise [25]. At the same time, in a real situation it is desirable to reduce the rate of numerical calculations, i.e., to apply the perturbation only infrequently. We propose the optimal way of control when the perturbation is applied not at each step but at some specific dangerous points. This can be done due to the above-mentioned inhomogeneity of the trajectories in the phase space. We avoid unnecessary calculations of the perturbation (12) at the points where the probability of deviation from the target trajectory is weak, but take special care at the dangerous points, where such probability is high.

The first question that arises is how to locate UPO's, which are the object of control. Traditional methods of locating periodic orbits based on the Newton-Raphson procedure require a good guess of the initial conditions for the iterative procedure. In general, they are not applicable for cycles with high periods. An appropriate general method was developed by Schmelcher and Diakonos [27]. The method is applicable even for the least unstable high-period orbits [28]. They used the principal idea of control—transforming unstable orbits into stable ones—to locate UPO. The first step of the method [27] is to apply a universal linear transformation of coordinates in order to get stable orbits at the same positions where unstable orbits are located. Then the position of stable orbits in new coordinates can be found by a simple iterative procedure. For the 2D case the transformation of coordinates takes the following form:

$$\mathbf{r}_{n+1}=\mathbf{r}_n+\mathbf{\Lambda}_i[\mathbf{F}^k(\mathbf{r}_n)-\mathbf{r}_n], \tag{13}$$

where $\mathbf{\Lambda}_i$ is one of $\alpha_2=8$ ($i=1,2,\ldots,8$) invertible 2×2 matrices. (In D-dimensional space there $\alpha_D=D!2^D$.) The concrete form of Λ_i is determined by the type of the *corresponding* unstable fixed point. In Figs. 7(a)–7(d) an example of this transformation for some points of high-period ($k=34,35$) UPO is shown. We used the transformation (13) with the matrix $\mathbf{\Lambda}=\left(\begin{smallmatrix}1 & 0\\ 0 & -1\end{smallmatrix}\right)$ in order to locate a hyperbolic point [see point *c* in Fig. 7(a)]. This transformation converts a hyperbolic fixed point into a stable focus. Iterating Eq. (13), starting from an arbitrary place near point *c*, after

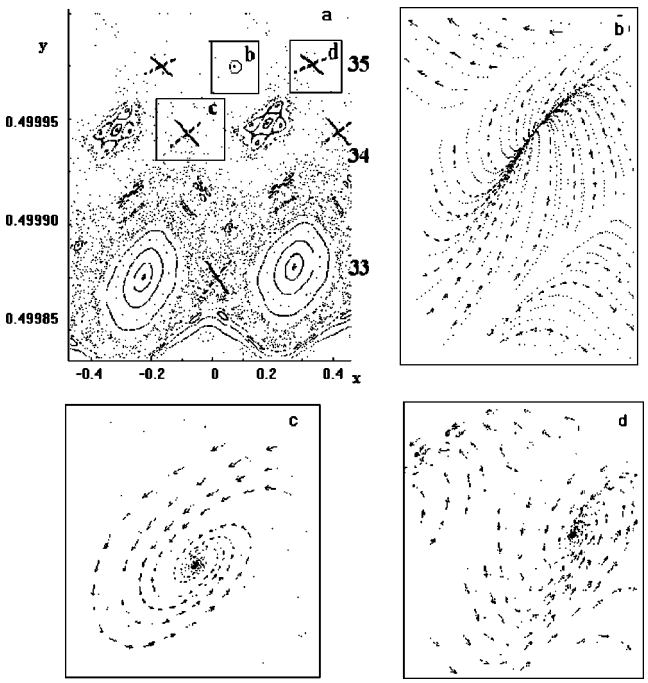

FIG. 7. Evolution of the phase space under transformation Eq. (13), shown for some points of the UPO's with $k=34$ and $k=35$. (a) Initial view of a small domain of the phase space. The elliptic point is marked by a circle within square *b* and the hyperbolic points are marked by crosses within squares *c* and *d*. Stable (unstable) directions at the hyperbolic points are shown by solid (dashed) lines. (b)–(d) Enlargement of the vicinity of the fixed points *b*–*d*, respectively, after the transformation Eq. (13).

10–20 iterations we reach the focus. Its location coincides with the hyperbolic fixed point *c*. Recently Davidchack and Lai [29] presented a method for the fast, complete, and accurate detection of UPO in chaotic systems. Their method is essentially based on the method by Schmelcher and Diakonis [27] and gives an effective technique for selection of the starting points.

In Fig. 8(a) we show the behavior of the deviation $\mathbf{r}_n-\mathbf{r}_n^*$ as the control is switched on and off. One can see that the system exhibits a long transient period before a trajectory can be stabilized. We use the logarithmic scale to separate different stages of the control procedure: (1) chaotic oscillations before entrapment under control; (2) an exponentially fast approach to the target periodic orbit; (3) stable motion along the unstable period-34 orbit; (4) exponentially fast deviation from the target orbit after the control is off; (5) reconstruction of natural chaotic oscillations. The rates of exponential approach (stage 2) and exponential deviation (stage 4) are different. The former is determined by the amplitude of external perturbation and the latter by the parameters of the free evolution of the system (in particular by the Laypunov exponent).

Figure 9 demonstrates the mechanism of OGY control in action. We launch four testing points (black squares) from the vicinity of randomly selected saddle points which belong to the period-34 orbit. The trajectories of the testing points are shown after three successive iterations. After the third iteration these points are aligned along the stable direction.

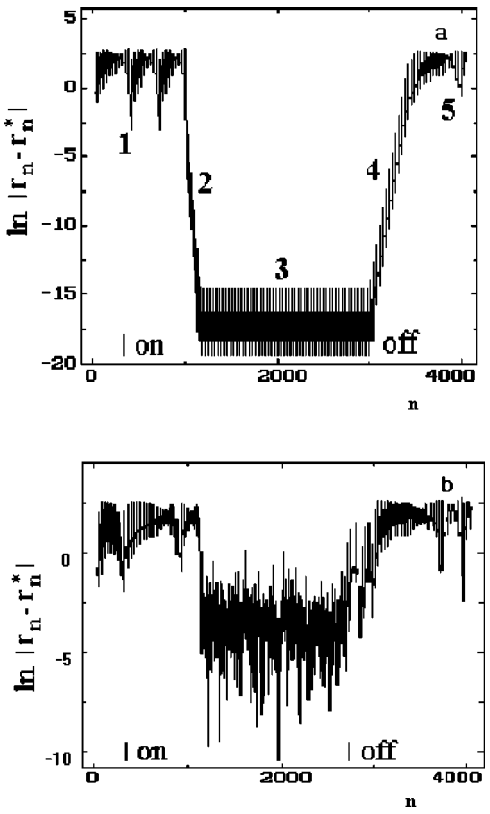

FIG. 8. Stabilization of the coordinate $\mathbf{r}_n$ when control is switched on: (a) without noise, (b) with Gaussian noise.

Then they follow the periodic orbit remaining in alignment and approaching the saddle point after each iteration.

At first glance it looks as though the results of the control of the high-period unstable orbit in reversible maps were very similar to the corresponding results for pure Hamiltonian systems [24]. Nevertheless, more careful examination shows that in reversible maps the coexistence of attractor and stability islands complicates the situation considerably. The point is that Eq. (12) is valid only when the trajectory $\mathbf{r}_n$ enters a region which is sufficiently close to the target periodic orbit. The size and the shape of this region [let us call it the entrapment region (ER)] are determined by the quantity δp_{max} and the local characteristics of a periodic orbit (**f**, **L**, and **B**). In our numerical study δp_{max} is taken from the interval 0.0007–0.03. In fact, OGY control relation (12) can be represented as follows:

$$\delta p_n = M_i \delta x_n + N_i \delta y_n, \quad i = (n) \bmod k. \tag{14}$$

The coefficients M_i and N_i can be obtained directly from Eq. (12). The ER for any ith point of the periodic orbit is determined by the condition

$$|M_i \delta x + N_i \delta y| < \delta p_{max}. \tag{15}$$

In Table I we give numerical values for the coefficients M_i and N_i in some typical points of the UPO. The size of the ER's determine the time of the entrapment under the control as well as the critical amplitude of noise which breaks down control. The area S_i of the ER for any point on the UPO is proportional to δp_{max}. The proportionality coefficient varies along the orbit and is given by the numbers M_i, N_i. For example, the coefficient M_i varies by 4 orders of magnitude along the orbit (see Table I). Then the sizes of the ER's of the corresponding points on the UPO also differ by a few orders of magnitude. Keeping this fact in mind, it is worthwhile to introduce a concept of *local* and *global* control for UPO with essentially different ER's. In the case of local control the condition $|\delta p_n| < \delta p_{max}$ is valid only at certain points of the periodic orbit. In the case of global control this condition is valid anywhere in the UPO. It is clear that the difference between local and global control practically vanishes if the orbit is a fixed point or a homogeneous orbit, i.e., an orbit with approximately equal areas of the ER for all points along the orbit. This occurs because if the entrapment condition is satisfied once (locally), it will also be satisfied at any other point of the UPO, thus leading to global control. In contrast,

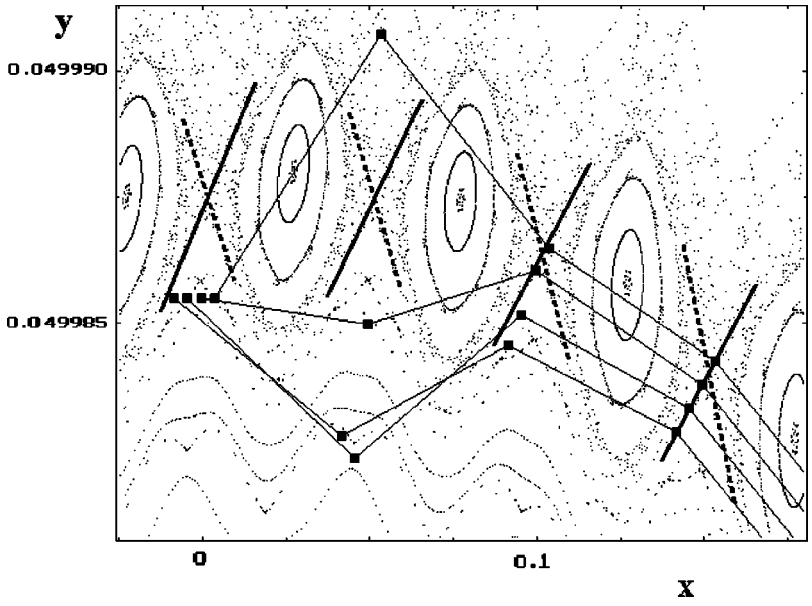

FIG. 9. Local evolution of four testing points towards the stable direction. Stable (unstable) directions are shown by solid (dashed) lines.

TABLE I. Size of the entrapment region for different points on the UPO.

Points	x^*	y^*	M_i	N_i
	3.4165	0.4997	−0.000 348	2.722
Close to the attractor (dangerous points)				
	3.9161	0.4996	−0.000 404	2.502
	5.6863	−1.9060	−2.556 355	2.034
Far from the attractor				
	1.4545	−4.2317	−3.396 934	5.044

for nonhomogeneous UPO, global control takes place only when the condition of local control for points with minimal areas of ER is satisfied. From the point of view of the realization of control, these points are *dangerous*. Figure 10 shows some specific features of the realization of control in the complex system (1). In Fig. 10(a) we show a transient region from the moment when the perturbation is turned on to the steady stage of global control. The duration of this transient region is about 700 iterations. In Fig. 10(b) we show the moments at which the condition of local control ($|\delta p_n| < \delta p_{max}$) was satisfied at any point of the controlled orbit. The role of the dangerous points can be seen in Figs. 10(c) and 10(d), where we plot the controlling perturbation δp_n for two dangerous points given in Table I. Numbers along the horizontal axis, $T = n/k$, is the discrete time n measured in units of the period of the orbit, $k = 34$. The amplitude of the controlling perturbation drops almost to zero as soon as the condition of the local control has been satisfied. After that moment the whole orbit is trapped under control. Unlike this, a multiple application of the controlling perturbation at the points which are not dangerous (the perturbation was turned on an average of once per period) does not provide a realization of global control. Some vertical lines in Figs. 10(b)–10(d) are thicker than the others. Thick lines

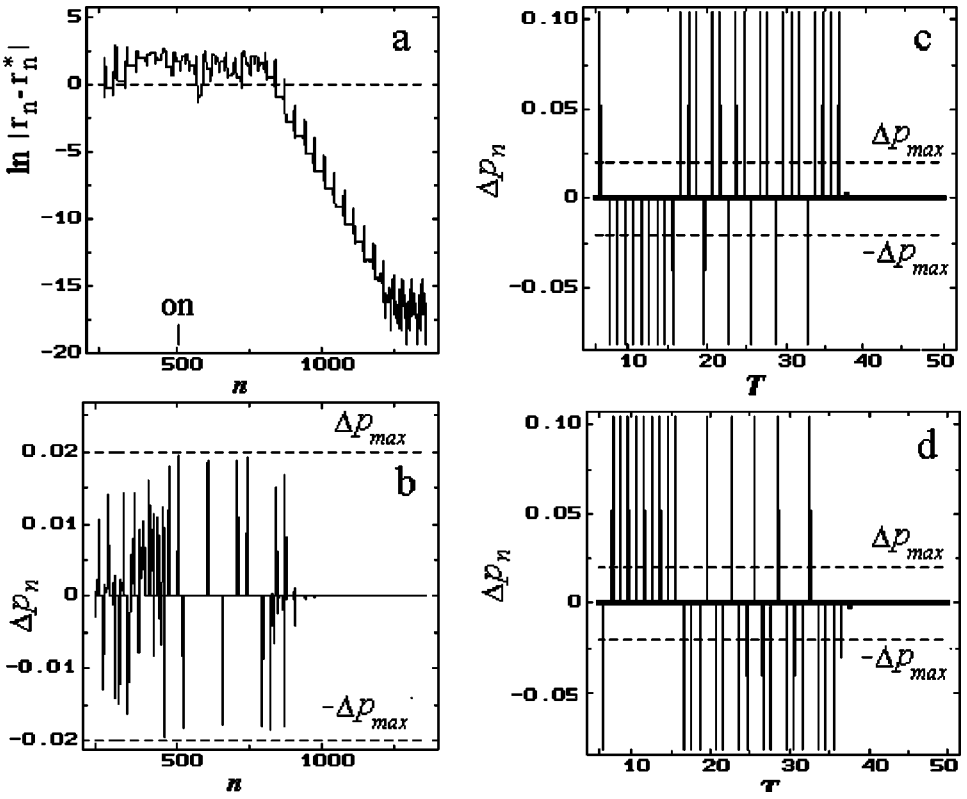

FIG. 10. (a) Transient behavior at the initial stage of control. The control perturbation is applied at the 500th iteration. About 300 iterations after that the trajectory is moving chaotically. Fast convergence to the target trajectory starts at around the 800th iteration. The transient phase is completed when the trajectory is stabilized near the target trajectory. Here the deviation from the target trajectory is reduced by almost 20 orders of magnitude in comparison with the initial chaotic trajectory. (b) Temporal variation of the controlling parameter δp_n [see Eq. (12)] along the same trajectory. Horizontal lines $\delta p_n = \pm \delta p_{max}$ show the interval where the condition of local control is satisfied. It is clearly seen that while this condition has been satisfied many times, control is not established. (c) and (d) Controlling perturbation δp_n ($T = n/k$) for two dangerous points given in Table I. Global control is realized immediately after the condition of local control has been satisfied.

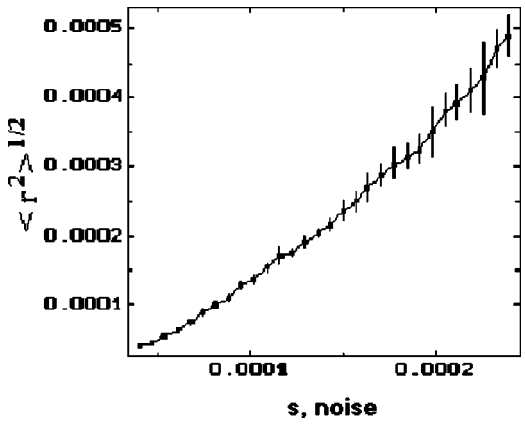

FIG. 11. Rms deviation from the target orbit vs amplitude of the external noise. This deviation shows the stability of control.

appear when the trajectory returns to the same point for the time interval which cannot be resolved in the horizontal axis scale. This may happen only before the global control is established.

To check the sensitivity of the control to external Gaussian noise we add a term $s\vec{\xi}_n$ to the right-hand side of Eq. (1). Here the components ξ_{x_n} and ξ_{y_n} are independent identically distributed random variables with zero mean value and a unit variance. In Fig. 8(b) we show the effect of the Gaussian noise with $s=0.01$. In the logarithmic scale one can clearly see that when subjected to the action of the noise the efficiency of control goes down by orders of magnitude. However, the OGY method even in the presence of noise allows control to be maintained during the same temporal interval as without noise.

We also study the effectiveness of control for different amplitudes s. The effectiveness can be characterized by the root-mean-square deviation $r(s)$ of the real trajectory from the target periodic orbit. The plot in Fig. 11 exhibits an almost linear dependence, $r(s)\propto s$ at low levels of noise. This dependence becomes nonlinear when the amplitude s increases. Such behavior is in agreement with recent theoretical estimations [30,31].

It is worth noting that the points which are marked as dangerous in the process of global stabilization remain dangerous as well with respect to the breakdown of control in the presence of noise. At the dangerous points the condition of local control, $\delta p_n < \delta p_{max}$, is violated much more often than at points with large entrapment areas. For example, for amplitude $s=0.06$, the condition of local control was satisfied only 1 or 0 times in a total of 120 attempts ($120\times 34=4080$ iterations) at the dangerous points shown in Table I. At the points close to the attractor, however, the same condition was satisfied 119 times.

IV. CONCLUSIONS

We presented a study of the phase space of a complex system and propose a modified OGY method that enables us to control high-period unstable orbits. The dynamics of the complex system is described by mapping (1) and is essentially affected by the interaction between the attractor and the stability islands. This interaction gives rise to strong spatial and temporal inhomogeneity of the phase space. Because of this inhomogeneity a typical trajectory consists of regular parts (close to the attractor) and chaotic regions far away from it. In the chaotic region the trajectory exhibits intermittency, i.e., a diffusive motion along the y axis is suddenly interrupted by long jumps. When $y\rightarrow\pm\infty$ the diffusion becomes anomalously fast; here the root-mean-square displacement grows exponentially with time.

Because of all these singularities, which are typical for any complex system, a direct application of the OGY method to control high-period unstable orbits fails. Effective at every step of iteration, it nevertheless requires hard computational efforts to calculate stable and unstable directions at each point of the orbit. Another option—to apply the control perturbation at every kth step of the period-k orbit—is much easier from the point of view of calculations, but is unstable with respect to external noise. Our version of the OGY method is free from these difficulties. It was developed especially for systems with strongly nonhomogeneous phase space and is based on the concept of local and global control. We demonstrated that by applying OGY control only at dangerous points we obtain the same efficiency that the original OGY method has, but at the same time reduce drastically the computational efforts. For the above-considered example of the period-34 orbit the dangerous points constitute only $\approx 30\%$ of the total number of points at the periodic orbit. The concept of local and global control turns out to be sufficiently powerful and effective and makes it unnecessary to develop a new method of control different from the OGY method.

ACKNOWLEDGMENTS

This research was supported by the Fundamental Research Foundation of the Ukraine Ministry of Science, Grant No. 2.4/342, and by CONACyT (Mexico), Grant No. 28626-E.

[1] A. J. Lichtenberg and M. A. Liberman, *Regular and Stochastic Motion* (Springer-Verlag, New York, 1982).
[2] L. E. Reichl, *Transition to Chaos* (Springer-Verlag, New York, 1992).
[3] N. B. Abraham, J. P. Gollub, and H. L. Swinney, Physica D **11**, 252 (1984).
[4] B. V. Chirikov, Phys. Rep. **52**, 263 (1979).
[5] K. Tomita, Phys. Rep. **86**, 113 (1982).
[6] J. P. Eckman, Rev. Mod. Phys. **53**, 643 (1981).
[7] E. Ott, Rev. Mod. Phys. **53**, 655 (1981).
[8] M. Henon, Commun. Math. Phys. **50**, 69 (1976).
[9] V. I. Arnold and M. B. Sevryuk, *Nonlinear Phenomena in*

Plasma Physics and Hydrodynamics (Mir, Moscow, 1986).
[10] M. B. Sevryuk, in *Reversible Systems*, Lecture Notes in Mathematics Vol. 1211 (Springer, Berlin, 1986).
[11] A. Politi, G. L. Oppo, and R. Badii, Phys. Rev. A **33**, 4055 (1986); C. L. Pando, L. and G. A. Luna-Acosta, Opt. Commun. **114**, 509 (1995).
[12] T. Post, H. W. Capel, G. R. W. Quispel, and J. P. Van der Weele, Physica A **164**, 625 (1990).
[13] J. A. G. Roberts and G. R. W. Qwispel, Phys. Rep. **216**, 64 (1992).
[14] F. T. Arecchi, Nucl. Phys. B **2**, 13 (1987).
[15] V. Yu. Gonchar, P. N. Ostapchuk, A. V. Tur, and V. V. Yanovsky, Phys. Lett. A **152**, 287 (1991).
[16] V. Yu. Gonchar, E. Y. Svirinovskaya, A. V. Tur, and V. V. Yanovsky, Phys. Lett. A **174**, 421 (1993).
[17] L. Poon and C. Grebogi, Phys. Rev. Lett. **75**, 4023 (1995).
[18] E. Ott, C. Grebogi, and J. A. Yorke, Phys. Rev. Lett. **64**, 1196 (1990).
[19] Y.-C. Lai and C. Grebogi, Phys. Rev. E **54**, 4667 (1996).
[20] S. Boccaletti, C. Grebogi, Y.-C. Lai, H. Mancini, and D. Maza, Phys. Rep. **329**, 103 (2000).
[21] Yu. L. Bolotin, V. Yu. Gonchar, A. A. Krokhin, A. Tur, and V. V. Yanovsky, Phys. Rev. Lett. **82**, 2504 (1999).
[22] V. I. Arnold *Advanced Theory of Ordinary Differential Equations* (Moscow, Nauka, 1978) (in Russian).
[23] P. Manneville and Y. Pomeau, Physica D **1**, 219 (1980).
[24] Y.-C. Lai, M. Ding, and C. Grebogi, Phys. Rev. E **47**, 86 (1993).
[25] E. Ott, C. Grebogi, and J. A. Yorke, in *Chaos: Soviet-American Perspectives on Nonlinear Science*, edited by D. K. Campbell (American Institute of Physics, New York, 1990).
[26] Y.-C. Lai, T. Tél, and C. Grebogi, Phys. Rev. E **48**, 709 (1993).
[27] P. Schmelcher and F. K. Diakonos, Phys. Rev. Lett. **78**, 4733 (1997); Phys. Rev. E **57**, 2739 (1998).
[28] F. K. Diakonos, P. Schmelcher, and O. Biham, Phys. Rev. Lett. **81**, 4349 (1998); D. Pingel, P. Schmelcher, F. K. Diakonos, and O. Biham, Phys. Rev. E **62**, 2119 (2000).
[29] R. L. Davidchack and Y.-C. Lai, Phys. Rev. E **60**, 6172 (1999).
[30] R. Brown, N. F. Rulkov, and N. B. Tufillaro, Phys. Rev. E **50**, 4488 (1994).
[31] S. Haes, C. Grebogi, and E. Ott, Phys. Rev. Lett. **70**, 3031 (1993).